

Journal of Materials Chemistry A

Accepted Manuscript



This is an *Accepted Manuscript*, which has been through the Royal Society of Chemistry peer review process and has been accepted for publication.

Accepted Manuscripts are published online shortly after acceptance, before technical editing, formatting and proof reading. Using this free service, authors can make their results available to the community, in citable form, before we publish the edited article. We will replace this *Accepted Manuscript* with the edited and formatted *Advance Article* as soon as it is available.

You can find more information about *Accepted Manuscripts* in the [Information for Authors](#).

Please note that technical editing may introduce minor changes to the text and/or graphics, which may alter content. The journal's standard [Terms & Conditions](#) and the [Ethical guidelines](#) still apply. In no event shall the Royal Society of Chemistry be held responsible for any errors or omissions in this *Accepted Manuscript* or any consequences arising from the use of any information it contains.



Journal Name

ARTICLE

Generalized Synthesis and Evaluation of Formation Mechanism of Metal Oxide/Sulfide@C hollow spheres

Arka Saha,^a Pankaj Bharmoria,^a Aniruddha Mondal,^a Subhash C. Ghosh,^a Sourindra Mahanty^{*b} and Asit Baran Panda^{*a}

Received 00th January 20xx,
Accepted 00th January 20xx

DOI: 10.1039/x0xx00000x

www.rsc.org/

Herein, we report a generalized novel soft template approach for the synthesis of a variety of uniform metal oxides (MoO₂, Fe₃O₄, V₂O₃) and sulfides (MoS₂, ZnS)@C hollow spheres using sucrose and CTAB as soft template. The synthesized hollow spheres are uniform in size, with a size range of 800 nm to 1.3 μm. The developed methodology gives the opportunity to alter the carbon content just by varying the amount of sucrose in the precursor solution. The formation mechanism of soft template has also been studied through isothermal titration calorimetric (ICT), IR analysis and SEM of intermediate. The developed strategy is based on the *in-situ* formation of spherical soft template by the interaction of sucrose and CTAB under the experimental conditions; formation of inorganic shell by the interaction of metal salt and template surface; carbonization of sucrose under hydrothermal condition and finally formation of desired metal oxide/sulphide@C through calcination under 5% H₂ in N₂ flow. Performance of the synthesized MoS₂@C hollow sphere as anode for lithium-ion battery has also been examined to see the applicability of the developed procedure, as a typical representative and exhibited high specific capacity (~1100 mAhg⁻¹ at 150 mA g⁻¹) as lithium-ion battery anode.

Introduction

Owing to their porous structure, high surface area, inner hollow architectures and low density, micro/nano hollow structures have attracted tremendous attention in recent years.¹⁻² These materials find potential application in photonics, catalysis, sensor, drug delivery and energy conversion and storage system for their unique and improved properties.²⁻⁷ Till date, remarkable progress has been made on hollow structure synthesis and a number of chemical and physicochemical approaches have been established, which includes template method, Kirkendall effect, Ostwald ripening, self-assembly techniques and spray drying method.³⁻¹⁶ Among these, the template assisted method, such as hard templates (e.g., polymer latex, carbon, and anodic aluminum oxide templates)^{6, 8} and soft templates (e.g., supramolecular, ionic liquids, surfactant, and organogel)^{3-4, 9} has established to be the most effective way to produce hollow structures. Template method is based on the formation of core-shell structure by coating of desired material or its precursor on the surface of template, followed by removal of template by an appropriate technique. Hard template based methods are pursued most commonly due to their effectivity towards the production of

uniform hollow structures and applicability towards large variety of materials.^{6, 8} However, the procedure is expensive and needs additional steps to synthesize as well as removal of templates, and there is a probability to break the hollow architectures during template removal. On the other hand, soft template methods are simple and inexpensive, templates are formed *in-situ* and easy to remove by simple solvent extraction process. But, it is highly challenging to get the uniform hollow structure using this method. Although there are number reports on the synthesis of uniform hollow spheres by soft template, but the methods are materials specific.^{3,10,12} Based on our knowledge, there are no literature reports on the development of generalized soft template synthetic strategy for hollow spheres of different materials, which is extremely demanding and essential to have. Thus, development of such a method for the synthesis of uniform inorganic hollow spheres is still remain a challenge.

Recent studies reveal that use of nanostructured materials with specific morphology may not be the ultimate solution for some particular application, such as capacitor, anode material for the next generation LIBs. In this regard, carbon based nano-composites, active-inactive material, in combination with desired morphology showed excellent reversibility, as the so-called electrode pulverization and loss of inter particle connectivity for volume expansion during cycling, could be overcome.¹⁴⁻¹⁵ However, reports on carbon incorporated hollow spheres are rare. Wu *et al.*¹⁶ synthesized SnO₂@C hollow sphere by a multi-step kirkendall method, Qiu *et al.*¹⁷ reported the phosphorus-doped graphene-wrapped MoS₂ hollow spheres through a post synthesis incorporation of

^a Central Salt and Marine Chemicals Research Institute (CSIR-CSMCRI) and CSMCRI-Academy of Scientific and Innovative Research, G. B. Marg, Bhavnagar-364002, Gujarat, India. E-mail: abpanda@csmcri.org.

^b CSIR-Central Glass & Ceramic Research Institute, Raja S C Mullick Road, Kolkata-700032, India. E-mail: mahanty@cgcri.res.in

Electronic Supplementary Information (ESI) available: [experimental procedure, additional XRD, TEM, SEM images, and TG curve]. See DOI: 10.1039/x0xx00000x

graphene. Thus, soft template method may be the unique procedure for the synthesis of carbon incorporated hollow sphere using the template as carbon source and the probability of breaking of hollow structure will be overcome. However, the reported soft template methods did not give the opportunity to tune the carbon content. Further, for the formation of uniform hollow spheres of different materials, it is essential to understand the interaction between the molecules and ions present in the reaction system, and in-turn the formation mechanism.

Herein, we report a generalized soft template approach for the synthesis of carbon incorporated uniform metal oxide (MoO_2 , Fe_3O_4 , V_2O_3) and sulphide (MoS_2 , ZnS) hollow spheres with a flexibility to control over the carbon content using corresponding aqueous solution of metal salt as metal source, potassium ethyl xanthogenate as sulphur source, and CTAB and sucrose as a combined template material as well as carbon source under basic condition. The corresponding formation mechanism of spherical soft template as well as hollow spherical structure is also evaluated by isothermal titration calorimetric analysis, IR, and SEM of intermediate, for the first time.

Experimental

Materials

Analytical grade ammonium heptamolybdate tetrahydrate [$(\text{NH}_4)_6\text{Mo}_7\text{O}_{24} \cdot 4\text{H}_2\text{O}$, 99.98%], cetyltrimethyl-ammonium bromide (CTAB, Sigma-Aldrich), potassium ethyl xanthogenate ($\text{C}_3\text{H}_5\text{KOS}_2$) were purchased from Sigma-Aldrich, zinc(II) Nitrate hexahydrate [$\text{Zn}(\text{NO}_3)_2 \cdot 6\text{H}_2\text{O}$], ammonium metavanadate (NH_4VO_3), Sucrose ($\text{C}_{12}\text{H}_{22}\text{O}_{11}$), Ammonium carbonate (NH_4HCO_3 & $\text{NH}_2\text{CO}_2\text{NH}_4$) were obtained from s.d.Fine, India, and Iron(II) Sulphate heptahydrate ($\text{FeSO}_4 \cdot 7\text{H}_2\text{O}$), Ethanol extra pure ($\text{C}_2\text{H}_5\text{OH}$) were purchased from SRL, India. All the chemicals were used as received without further purification. Water, obtained from a Millipore water purifier, with a resistivity of 18MU cm was used for all the reactions.

General synthetic procedures

In a simple generalized synthetic procedure, CTAB was dissolved in deionised water with constant stirring. After that sucrose was added to the solution. Sucrose binds with CTAB through electrostatic and H-bonding interaction. The amount of sucrose was varied and in three different sets 0.228 g., 1.0910g; 2.06 g of sucrose was used with respect to 0.1948 g of CTAB. After that we added aqueous solution of metal salt precursors and/or Potassium ethyl xanthogenate (for sulphide only) as sulphur sources. In this stage addition of little amount of ammonium hydroxide was needed for adjustment of pH to 10 for metal sulfides. After stirring the resultant solution for 10 min, 33ml of the obtained turbid solution was transferred to a 50 ml Teflon-lined stainless steel autoclave and sealed tightly, heated at 130 °C for 12 h, followed by 220 °C for 12 h. After cooling naturally, the obtained precipitate was collected,

washed with deionised water followed by ethanol, dried at 70 °C for 24 h and calcined at desired temperature in a stream of 5% H_2 and 95% N_2 at a scan speed of 5 °C / min. The MoS_2/C composite were obtained after calcination of the dried material at 800 °C for 5h. The samples synthesized with 0.228 g, 1.0910g, 2.06 g of sucrose were named as 1, 2, and 3. Specifically for MoS_2 , the corresponding samples are $\text{MoS}_2/\text{C}-1$, $\text{MoS}_2/\text{C}-2$ and $\text{MoS}_2/\text{C}-3$. For detailed experimental procedures for individual material please see ESI[†], detailed experimental procedure.

Characterizations.

Powder X-ray diffraction patterns were recorded in the 2 θ range of 2-80° on a Philips X'pert X-ray powder diffractometer using $\text{Cu K}\alpha$ ($\lambda = 1.54178 \text{ \AA}$) radiation. Thermo gravimetric analysis (TGA) was performed on Mettler-Toledo (TGA/SDTA 851e) in air at a heating rate of 10 °C/min. The nitrogen adsorption - desorption measurements at 77 K were performed on ASAP 2010 Micromeritics, USA, after degassing samples under vacuum (10-2 torr) at 250 °C for 4 h. The surface area was determined by Brunauer-Emmett-Teller (BET) equation. Pore size distributions were determined using BJH model of cylindrical pore approximation. A scanning electron microscope (SEM) (Leo series 1430 VP) equipped with INCA was used to determine the morphology of samples. The sample powder was supported on aluminum stubs and then coated with gold by plasma prior to measurement. Transmission electronic microscope (TEM) images were collected using a JEOL JEM 2100 microscope and samples were prepared by mounting an ethanol dispersed samples on lacey carbon formvar coated Cu grid. The obtained average size of the CTAB- sucrose solution through DLS measurement were recorded in Malvern instrument (Zetasizer, Nano series, Nano-ZS90). Calcination of the powdered samples was carried out in High Temperature Vacuum Tube Furnace (MTI, OTF-1200X). Isothermal calorimetric titration was carried out in Microcal iTC200.

Electrochemical measurements.

Electrochemical properties of the synthesized hollow sphere shaped MoS_2/C nanoparticles were evaluated in 2032 type coin cells vs Li/Li+. A typical electrode was prepared from a slurry consisting of MoS_2/C nanoparticle powder (70 wt%), acetylene black (20 wt%) and PVDF binder (10 wt%) in *n*-methyl pyrrolidinone (NMP) solvent. The slurry was coated onto a 15 μm thick copper foil (current collector) and dried at 110°C in an oven for 12 h. After pressing the coated foil at 4.0 ton inch^{-2} , circular disks of 15 mm in diameter were cut and used as electrode. Typical weight of the active material (excluding acetylene black and PVDF) was 3-5 mg. Coin cells were assembled with these electrodes using Li metal as counter as well as reference electrode, LiPF_6 in EC: DMC (1:2 vol%) as electrolyte and Celgard 2300 as separator within an argon filled glove box (M'BRAUN, Germany) where the moisture and oxygen levels were both kept below 1.0 ppm. Gavanostatic charge-discharge measurements were carried

out using an automatic battery tester (Model: BT2000, Arbin, USA) in the potential window of 0.01- 3.0 V with a constant current density of 50 mA g^{-1} for the initial formation cycle and at different current densities ranging from 150 mA g^{-1} to 1.0 A g^{-1} for subsequent cycles. Same current density was for both discharge and charge in every case. Cyclic voltammetry was performed with a galvanostat-potentiostat (Model: PGSTAT 302N, Autolab, the Netherlands) in the potential window of 0.01-3.0 V at a scan rate of 0.1 mVs $^{-1}$. Electrochemical impedance spectroscopy (EIS) measurements were carried out with the same galvanostat-potentiostat in the frequency range of 10 mHz-1.0 MHz at open circuit potential with an AC amplitude of 10 mV.

Results and discussion

The developed strategy is based on the formation of spherical soft template by the interaction of sucrose and CTAB under the experimental conditions; formation of inorganic shell by the interaction of metal salt and template surface; carbonization of sucrose under hydrothermal condition and finally formation of desire metal oxide/sulfide @C through calcination under 5% H $_2$ in N $_2$ flow (see ESI † , detailed experimental procedure). Corresponding metal sulfides were formed through the *in-situ* formation of metal-xanthate complex by the interaction of metal ion and xanthetic acid, followed by decomposition.¹⁸ Here it is essential to mentioned that during the synthesis the hollow spherical metal sulphides adjustment of pH through addition of ammonium hydroxide was need to facilitate the decomposition of *in-situ* formed metal-xanthate. In presence of ammonium group the decomposition of metal-xanthate to sulfide took place through a *Chugaev* like mechanism, involves a concerted three electron-pair shift.¹⁹ Amount of carbon was controlled by varying the amount of sucrose in the precursor solution. The

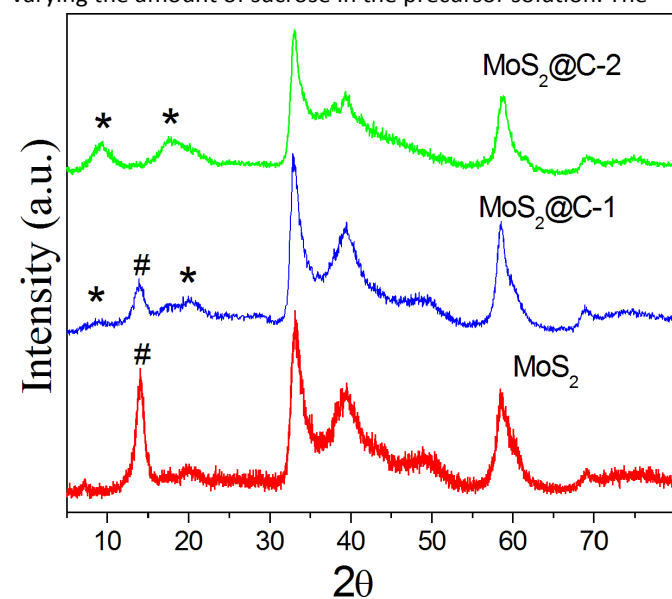


Fig. 1 X-ray diffraction pattern of synthesized MoS $_2$ with varying amount of carbon.

method was first demonstrated for the preparation of MoS $_2$ @C hollow sphere.

Fig. 1 represents the x-ray diffraction patterns of the synthesized MoS $_2$ with varying amount of carbon obtained after calcination for 5h at 800°C. XRD patterns exhibit well resolved diffraction peaks. The pattern of pure MoS $_2$ (without carbon) matched well with the JCPDS file (37-1492) of corresponding layered MoS $_2$, where the peak at $2\theta=14.2$ can be indexed to (002) confirming the formation of well stacked layered structure. However, in the XRD patterns of carbon incorporated MoS $_2$, the peak at $2\theta=14.2$ disappeared with the generation of two new peaks at around 9.3 and 17.8 ($d=0.9510$ nm and 0.4982 nm) keeping all other peak positions constant. This phenomenon indicated that the carbon was incorporated inside the MoS $_2$ layers, which increased the interlayer spacing and peak for (002) was shifted towards higher 2θ reason. Thus, the peak at 9.3 can be assigned to carbon incorporated exploded inter MoS $_2$ layer spacing. Whereas, the generated another new peak at $2\theta=17.8$ most probably due to the inter MoS $_2$ -carbon layer (Scheme S1, ESI †). Here it is essential to mentioned that the obtained XRD pattern of as-synthesized carbonized intermediates of MoS $_2$, obtained after hydrothermal treatment, are identical to that of calcined one and only observed difference are in there intensity. The intensity of peaks of calcined product are quite high with respect to that of just carbonized materials (Fig. 1& S1, ESI †). From the XRD results, it is evident that under hydrothermal conditions the crystallization of MoS $_2$ took place.

Fig. 2 represents the corresponding SEM images of as-synthesized carbonized intermediates, obtained after hydrothermal treatment, as well as calcined of MoS $_2$. The SEM

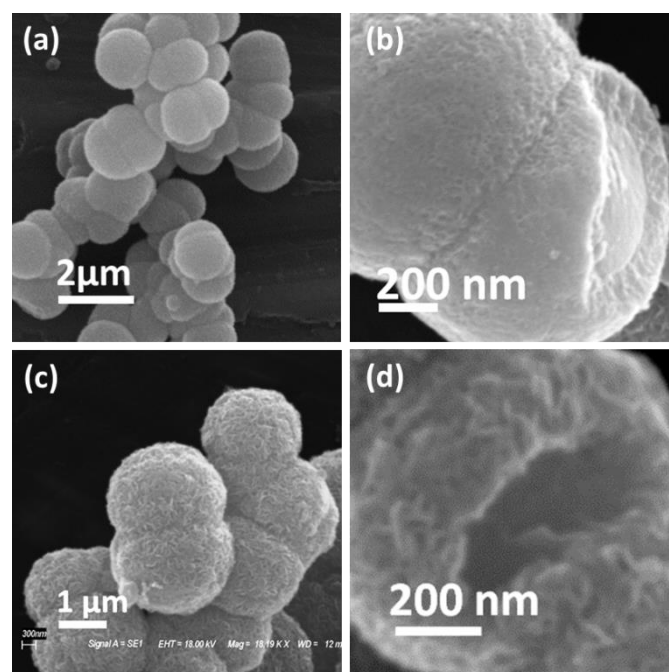


Fig. 2 SEM images of as-synthesized carbonized intermediates (a, b), obtained after hydrothermal treatment, and calcined (c, d) of MoS $_2$ @C-3.

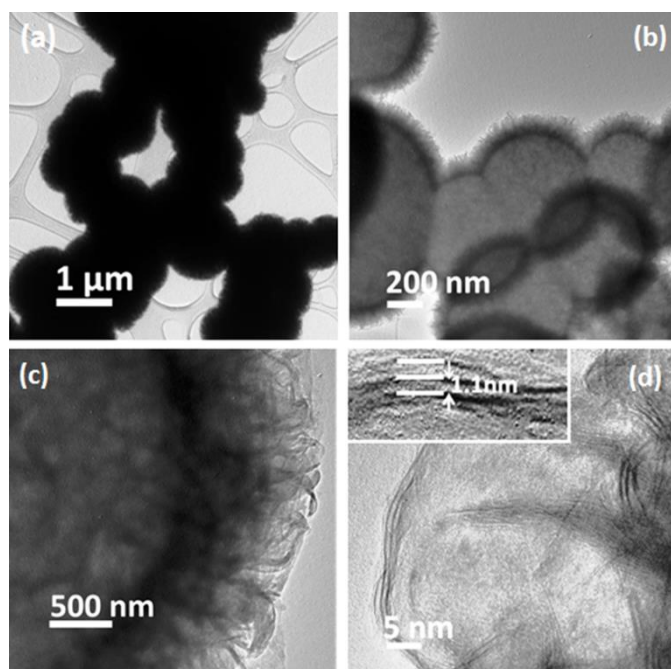


Fig. 3 TEM and HR-TEM images of as-synthesized carbonized intermediates, obtained after hydrothermal treatment, and calcined of MoS₂@C-3.

Image of as-synthesized MoS₂ indicates the formation of uniform spheres with a size range of 800 nm to 1.3 μm (Fig. 2a) and surface of the spheres are rough. In the broken part of the as-synthesized spheres, the presence of solid material in the inner part confirmed that as-synthesized spheres are solid and the observed thickness of outer coat are ~120nm (Fig. 2b). No such distinct morphological change was observed even after calcination, surface roughness became more prominent and it appear that the spheres were composed by flake-like subunits (Fig. 2c). However, the empty interior in some of the partially broken spheres, which are clearly observable in the Fig. 2d, confirmed the calcined MoS₂ spheres are hollow in nature. Here, it is essential to mentioned that no such distinct change in morphology and inner architecture was observed with the variation of sucrose content (Fig. S2, ESI[†]).

Fig 3 represents the TEM and HR-TEM images of synthesized MoS₂@C-3 architectures as typical representatives. The low-resolution TEM image (Fig. 3a), further confirmed that the synthesized MoS₂ architectures are spherical in nature with uniform size. The inner hollow architectures in the corresponding magnified TEM image (Fig. 3b) confirmed the formation of hollow spherical nanostructures with a shell thickness of ~70-80 nm and support SEM results, the observed thickness of outer surface in broken part. However, the decreased thickness of outer surface (~10-15nm) on calcination is most probably due to contraction. TEM images also evident that the synthesized MoS₂ materials are composed of nanosheets (Fig. 3b-c). A representative high-resolution transmission electron microscopy (HR-TEM) image of the MoS₂ nanostructures (Fig. 3d) shows the sheets are very thin and are composed of 2 to 5 stacking of MoS₂ layers. The observed inter-layer spacing of

~1.1nm, higher than that of the layer spacing of bare MoS₂ (inset Fig 3d and Fig. S3, ESI[†]). This can be perfectly assigned to the observation of a XRD peak at 2θ=9.3 and support the XRD result. Thermo-gravimetric (TG) curves of the synthesized carbon incorporated samples reveal the incorporation of 10 to 32 wt% of carbon depending upon the amount of sucrose (Fig. S4, ESI[†]), specifically it is 10% for MoS₂@C-1, 16% for MoS₂@C-2, 32% for MoS₂@C-3. The specific surface area of MoS₂@C materials was increased with the increase in the carbon contentment and it was 73 m²g⁻¹ for MoS₂@C-3. Corresponding XPS study of MoS₂@C-3 reveals the presence of Mo⁴⁺ with very little amount of Mo⁶⁺, S²⁻ and carbon with certain extent of graphitic carbon. XPS also evidenced the good interaction of MoS₂ with carbon matrix (Figure S5, ESI[†]).

In the control reactions, materials synthesized in the presence of either CTAB or sucrose alone produced only random particles; no spherically assembled particles could be observed (Fig. S6, ESI[†]). The control reaction confirmed the presence of both CTAB and sucrose together is crucial for the formation of spherical assembly as a template and in turn, the hollow sphere. Thus, it is essential to evaluate the exact formation mechanism of the synthesized hollow sphere. In the performed experimental concentration (15 mM sol), CTAB formed wormlike assembly of micelles.²⁰ It is assumed that the random wormlike micellar assembly was transformed to spherical assembly after addition of sucrose, through sucrose-CTAB interaction. DLS measurement confirmed that the average size of the spheres is ~300 to 700 nm with a mean size of 500nm (Fig. S7, ESI[†]). We failed to get the size of the product after addition of metal precursor, due to turbidity. However, it is logical to assume that the size would increase through metal ion-template interaction, as the sizes of the final spheres are higher than that of the template. Thus, it is essential to understand the nature of sucrose-CTAB interaction, the position of sucrose and CTAB in the template and the template-metal precursor interaction.

The heat changes due to binding of sucrose to CTAB micelles and consequent binding of ammonium heptamolybdate tetrahydrate to CTAB-sucrose complex have been detected through isothermal titration calorimetric (ITC)

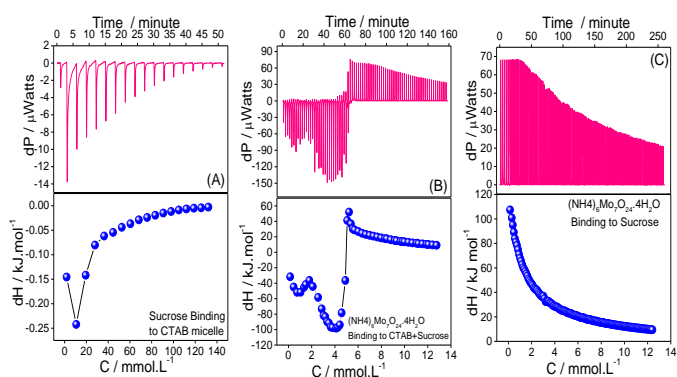
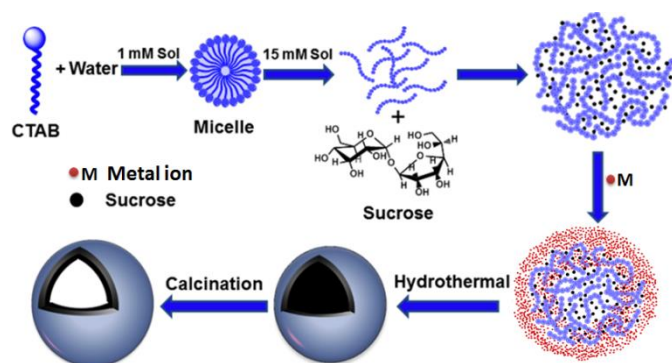


Fig. 4 Isothermal titration calorimetric binding enthalpograms and corresponding differential power plots of (a) Sucrose binding to CTAB micelle, (b) Ammonium heptamolybdate salt binding to CTAB-Sucrose complex and (c) Ammonium heptamolybdate salt binding to Sucrose.

analysis. Fig. 4 represent the enthalmograms and corresponding differential power plots derived from the interaction and subsequent binding of sucrose to CTAB micelles for template formation and then, binding of molybdate salt to the template. In the studied concentration, exothermic enthalpy changes were observed during binding of sucrose to CTAB micelles (Fig. 4a). Having positively charged ammonium head group at the surface of micelles, sucrose is likely to be bound to CTAB micelles via ion dipole interactions of its oxygen atoms or via hydrogen bonding of sucrose O-H group and electron deficient nitrogen atom of CTAB head group. The curve shows that maximum binding occurs up to 80mM on addition of sucrose, as enthalpy changes became almost constant thereafter. The binding of molybdate to CTAB-sucrose template is a two-step process (Fig. 4b). It can be presumed that the molybdate binds to both CTAB micelle and sucrose sequentially. The initial exothermic enthalpy changes can be assigned to the binding of molybdate to the CTAB micelles via attractive electrostatic interaction between ammonium head group of CTAB and molybdate ion. The initial minima observed in the curve may be due to the competitive binding of molybdate with ammonium head group of CTAB and free ammonium ion in the reaction system. The CTAB sites became saturated with molybdate after the addition of 5 mM of molybdate. Beyond 5 mM, the molybdate binds to the sucrose molecules of the template. The binding process of molybdate to sucrose is a highly endothermic in nature. The molybdate binding to sucrose in CTAB-sucrose complex has further been validated by studying the binding isotherm of salt to sucrose separately (Fig. 4c). Although there is a difference in actual enthalpy values (which might be due the presence of CTAB in CTAB-sucrose template) but the binding behaviour is similar. The hydrogen bindings in sucrose-CTAB system have been further supported by the FT-IR spectra (Fig. S8, ESI[†]). A weak hydrogen bonding was observed between sucrose O-H group and CTAB nitrogen atom due to steric hindrance as evidenced by the decrease in $\nu_{\text{O-H}}$ at 3391 cm^{-1} by 1 cm^{-1} and $\nu_{\text{O-H}}$ at 3564 cm^{-1} by 2 cm^{-1} upon binding to CTAB micelles. Upon addition of the salt these vibration bands disappeared and overlap band of N-H stretching vibrations of the ammonium group of added salt and sucrose O-H appeared at 3396 cm^{-1} .



Scheme 1 Proposed step wise formation mechanism of hollow sphere based on the experimental findings and controlled reactions.

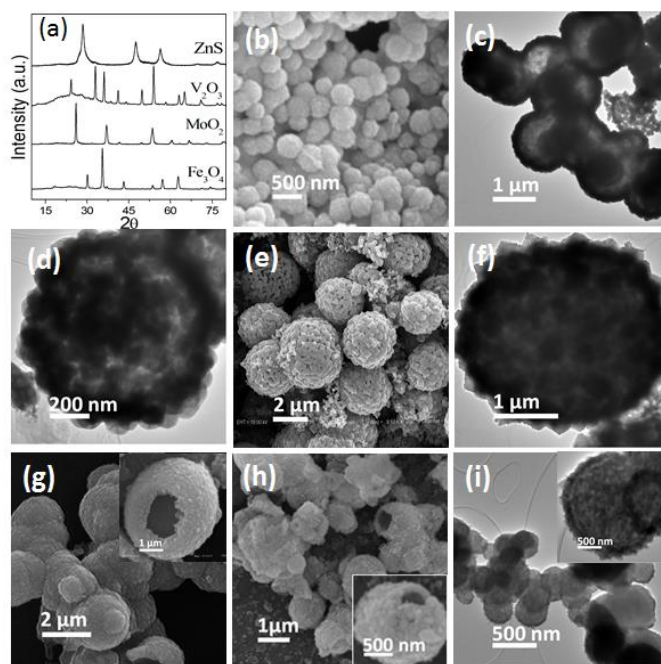


Fig. 5 (a) X-ray diffraction patterns of the synthesized hollow spheres and corresponding SEM and TEM images of the synthesized MoO₂ (b-d), Fe₃O₄ (e-f), V₂O₅ (g), and ZnS (h-i) hollow spheres.

Based on the above discussed observations on the simultaneous interaction of CTAB, sucrose and metal ion from isothermal titration calorimetric analysis and morphological and compositional observations from XRD, SEM, TEM and TG analysis, we have proposed a formation mechanism of MoS₂@C hollow sphere (Scheme 1). The mechanism is based on the formation of CTAB-sucrose-spherical architecture through interaction of wormlike CTAB micelles, formed in the reaction condition, and sucrose molecules, followed by deposition of metal salt on the surface of the spherical template and formation of carbonaceous solid sphere on hydrothermal treatment, which on calcination in 5% H₂ and 95% N₂ environment resulted the hollow sphere. Formation of carbonaceous solid sphere, as intermediate, is evidenced by the solid interior of broken outer surface (Fig. 2b). The sugar in the *in-situ* formed spherical soft template was carbonized on hydrothermal treatment and resulted solid spherical inner core.

After successful synthesis of MoS₂@C hollow spheres, we have extended the work to check the suitability of the developed synthetic strategy towards other hollow spherical metal sulfides, like ZnS, as well as metal oxides, like MoO₂, V₂O₅, Fe₃O₄. To our delight, we were able to synthesize phase pure carbon incorporated hollow spheres of the above mentioned metal sulfides and oxides (Fig. 5), following the similar methodology as adopted for MoS₂@C.

Fig. 5a represents the XRD pattern of the synthesized metal sulphides and oxides. The XRD pattern exhibit well resolved diffraction peaks which match well with the JCPDS file of corresponding single phase MoO₂ (JCPDS no. 32-0671), Fe₃O₄ (JCPDS no. 86-1354); V₂O₅ (JCPDS no. 85-1411) and ZnS

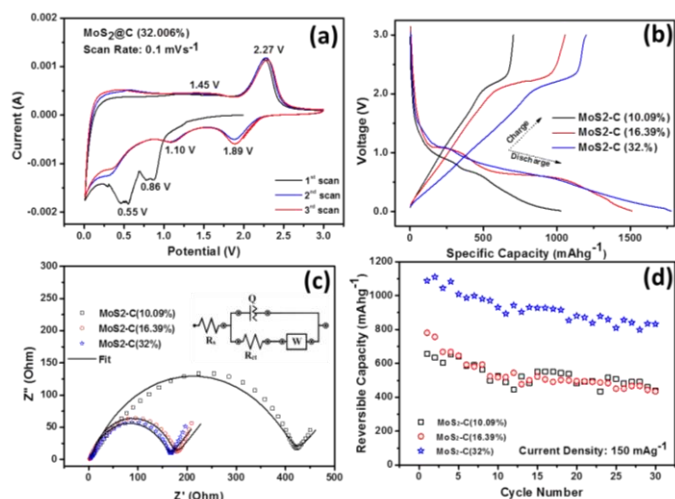


Fig. 6 Electrochemical properties of synthesized MoS₂@C hollow spheres: cyclic voltammetry (a), initial discharge charge profiles (b), Nyquist plots of as-assembled cells (c), and cycling behavior (d).

(JCPDS no. 05-0566) and confirmed the formation of phase pure materials. The surfaces of the spheres are rough. SEM images of all the synthesized materials indicates the formation of uniform spheres with rough surface (Fig. 5b,e,g&h). Hollow interior of the broken spheres indicate the formed spheres are hollow in nature. In the TEM images further confirmed the formation of uniform spheres and the low-contrast in the inner region of spheres confirmed that the synthesized spheres are hollow (Fig. 5c,d,f&i). Unlike MoS₂, the spheres are constructed of small individual nanoparticles instead of sheet. To see the applicability of the developed procedure, one of the synthesized materials, MoS₂, has been examined as an anode for lithium-ion battery by fabricating coin cells vs Li/Li⁺. MoS₂ is selected due to its unique diverse properties which find application in a wide range of fields.²¹⁻²² Recent results suggest that truly nanoscale structures containing a nanodispersed carbon phase can offer high charge storage capacities far exceeding the theoretical value of MoS₂, 669 mAhg⁻¹ (calculated on the basis of conventional intercalation/conversion reactions involving 4-electron transfer process).²³ Here carbon is shown to play a dual role: provides more conduction pathways improving the electrical conductivity of MoS₂ and induces a synergistic effect.^{14, 22-26} It has been found that carbon content in the range 28-50 wt% produces the best results and capacity values of 926-1214 mAhg⁻¹ have been reported.^{14, 24-27} Thus, it is reasonable to expect that the hollow sphere MoS₂@C nanoparticles with carbon content 10 to 32 wt%, synthesized in the present study, would show good charge storage ability. Here it is essential to mentioned that the yet reported pure and carbon incorporated MoS₂ hollow architectures are not good except the report of Wang *et al.*²⁸ and Qiu *et al.*¹⁷.

Fig. 6a shows typical CV curves of MoS₂@C (32%) for the first three cycles at a scan rate of 0.1 mVs⁻¹ in the potential window of 0.01–3.0 V. In the first cycle, the discharge process

starts with lithiation by intercalation (reduction peaks at 1.89, 1.10, and 0.86 V) which is accompanied by a phase transformation from 2H-MoS₂ (Mo in trigonal prismatic coordination) to 1T-LixMoS₂ (Mo in octahedral coordination),²⁹ followed by a conversion reaction (a sharp reduction peak at 0.55 V) yielding molybdenum nanoparticles (Mo) and lithium sulfide (Li₂S). In the anodic sweep, delithiation occurs through partial oxidation of Mo to form MoS₂ (1.45 V) and formation of polysulphur (2.27 V).^{25, 30} The initial discharge-charge profiles of MoS₂@C (Fig. 6b) at 50 mA g⁻¹ show that the discharge capacity increases with increasing carbon content. This can be related to the observance of decreased charge transfer resistance with increasing carbon content as deduced from the Nyquist plots (Fig. 6c & Table S1, Supporting Information) obtained from impedance spectroscopy measurements. The discharge/charge capacities in the first cycle have been found to be 1026/704 and 1512/1055 and 1778/1200 mAhg⁻¹ respectively for MoS₂@C (10%), MoS₂@C (16%) and MoS₂@C(32%) with coulombic efficiencies in the range 67-69%. However, in the subsequent cycles, the coulombic efficiency approaches unity for all samples indicating excellent reversibility. Interestingly, cycling performance (Fig. 6d), tested at a current density of 150 mA g⁻¹, shows similar capacity values (~500 mAhg⁻¹) for carbon content up to 16. But when the carbon content is increased to 32%, very high reversible capacity of 1086 mAhg⁻¹ is observed in the first cycle, ~80% of which is retained after 30 cycles even at the relatively high rate of 150 mA g⁻¹. To further test the rate performance, the cell was cycled at different current densities (Fig. S9, see ESI[†]). Even at a very high current density of 1 Ag⁻¹, steady capacity of ~480 mAhg⁻¹ could be observed. Such excellent performance could be attributed to the minimized Li⁺ diffusion distance, decreased polarization due to presence of carbon and large surface area of the synthesized nanoparticles with hollow spherical morphology. These values are comparable to the best results reported so far where preferably carbon nanotube / graphene were used in most of the cases to get the better results.²⁴⁻²⁷ Nonetheless, these initial results demonstrate an example of the potential applicability of the present strategy to synthesize metal oxide/sulphide@C hollow spheres. Here it is essential to mentioned that further increment of carbon content from 32% the electrochemical performance was decreased, most probably due to the increase in the amount of inactive material carbon.

Conclusions

In summary, we have developed a novel generalized sucrose-CTAB based soft template synthetic protocol for carbon incorporated metal oxide/sulphide hollow spheres and the developed strategy gives the opportunity to tune the carbon content just by varying the amount of sucrose in the precursor solution. The hollow spheres synthesized by the method are phase pure and uniform in size which remains in the size range of 800 nm to 1.3 μm. Mechanistic study based on interaction of CTAB, sucrose and metal ion by (ICT) analysis, DLS IR analysis, SEM image of intermediate and final product depict

that initially spherical CTAB- sucrose templet were formed and then formation of inorganic shell in the surface of template took place through the interaction of metal salt and template. Finally, hydrothermal carbonization of sucrose followed by calcination resulted the desired hollow sphere. The synthesized MoS₂@C hollow spheres, with 30%C, exhibited very high reversible capacity of 1086 mAhg⁻¹ in the first cycle, ~80% of which is retained after 30 cycles even at the relatively high rate of 150 mAhg⁻¹. The result is comparable with the best reported results. Finally, the developed protocol is unique, applies to the synthesis of a large variety of hollow sphere with improved properties and synthesized materials can be utilize for other applications.

Acknowledgements

CSIR-CSMCR I Communication No. 021/2015. Authors like to acknowledge DST, India (SR/S1/IC-33/2011) for financial support. AS acknowledge UGC, India, for a fellowship. The authors also acknowledge the "ADCIF" of CSMCR I for providing instrumentation facilities. SM and ABP thank Director, CSIR-CGCR I for kind permission to publish this work.

Notes and references

- J. Hu, M. Chen, X. Fang and L. Wu, *Chem. Soc. Rev.*, 2011, **40**, 5472; G. Zhang and X. W. Lou, *Angew. Chem. Int. Ed.*, 2014, **53**, 9041; Y. Zhao and L. Jiang, *Adv. Mater.*, 2009, **21**, 3621; Z. Wang, L. Zhou and X. W. Lou, *Adv. Mater.*, 2012, **24**, 1903; X. Lai, J. E. Halpert and D. Wang, *Energy Environ. Sci.*, 2012, **5**, 5604.
- M. Chen, C. Ye, S. Zhou and L. Wu, *Adv. Mater.*, 2013, **25**, 5343.
- S. Peng, L. Li, H. Tan, R. Cai, W. Shi, C. Li, S. G. Mhaisalkar, M. Srinivasan, S. Ramakrishna and Q. Yan, *Adv. Funct. Mater.*, 2014, **24**, 2155; J. Qi, K. Zhao, G. Li, Y. Gao, H. Zhao, R. Yu and Z. Tang *Nanoscale*, 2014, **6**, 4072; A. K. Sinha, M. Basu, M. Pradhan, S. Sarkar and T. Pal, *Chem. Eur. J.* 2010, **16**, 7865.
- Z. Yang, Z. Li, Y. Yang and Z. J. Xu, *ACS Appl. Mater. Interfaces*, 2014, **6**, 21911.
- Y. Li and J. Shi, *Adv. Mater.*, 2014, **26**, 3176.
- M. P. Lorenzo, B. Vaz, V. Salgueiri and M. A. C. Duarte, *Chem. Eur. J.*, 2013, **19**, 12196; R. Lv, P. Yang, Y. Dai, S. Gai, F. He and J. Lin, *ACS Appl. Mater. Interfaces*, 2014, **6**, 15550; G. Yang, S. Gai, F. Qu. and P. Yang, *ACS Appl. Mater. Interfaces*, 2013, **5**, 5788.
- M. Luo, Y. Liu, J. Hu, H. Liu and J. Li, *ACS Appl. Mater. Interfaces*, **2012**, **4**, 1813; X. Li, X. Liu, Y. Ma, M. Li, J. Zhao, H. Xin, L. Zhang, Y. Yang, C. Li and Q. Yang, *Adv. Mater.*, 2012, **24**, 1424.
- D. A. J. Herman, S. Cheong, M. J. Banholzer and R. D. Tilley, *ChemComm.*, 2013, **49**, 6203; D. Chen, L. L. Li, F. Q. Tang, S. O. Qi, *Adv. Mater.*, 2009, **21**, 3804; Z. Wang, Z. C. Wang, S. Madhavi, X. W. Lou, *Chem. Eur. J.*, 2012, **18**, 7561; X. Li, R. Huang, Hu. Yanhua, Y. Chen, W. Liu, R. Yuan and Z. Li, *Inorg. Chem.*, 2012, **51**, 6245; Y. Su, R. Yan, M. H. Dan, J. X. Xu, D. Wang, W. Q. Zhang and S. G. Liu, *Langmuir*, 2011, **27**, 8983; S. T. Tong, L. Mao, X. H. Zhang and C. Q. Jia, *Ind. Eng. Chem. Res.*, 2011, **50**, 13825.
- M. Sasidharan and K. Nakashima, *Acc. Chem. Res.*, 2014, **47**, 157; H. Zhou, T. Fan, D. Zhang, Q. Guo and H. Ogawa., *Chem. Mater.*, 2007, **19**, 2144; Y. Y. Xu, D. R. Chen, X. L. Jiao and K. Y. Xue, *J. Phys. Chem. C*, 2007, **111**, 16284; H. L. Xu and W. Z. Wang, *Angew. Chem., Int. Ed.*, 2007, **46**, 1489; M. Mazur, *J. Phys. Chem. C*, 2008, **112**, 13528; N. J. Carroll, S. Pylypenko, P. B. Atanassov and D. N. Petsev, *Langmuir*, 2009, **25**, 1354.
- A. Carne-Sanchez, I. Imaz, M. Cano-Sarabia and D. Maspoch, *Nature Chem.*, 2013, **5**, 203.
- C. C Yec and H. C. Zeng, *J. Mater. Chem. A*, 2014, **2**, 4843.
- Z. Wei, R. Xing, X. Zhang, S. Liu, H. Yu and P. Li, *ACS Appl. Mater. Interfaces*, 2013, **5**, 598.
- X. Kang, D. Yang, P. Ma, Y. Dai, M. Shang, D. Geng, Z. Cheng and J. Lin, *Langmuir*, 2013, **29**, 1286; B. Wang, H. We, L. Zhang and X. W. Low, *Angew. Chem. Int. Ed.*, 2013, **125**, 4259.
- K. Chang and W. Chen, *ACS Nano* 2011, **5**, 4720.
- J.-Y. Lin, C. Y. Chen and S. W. Chou, *Chem. Commun.*, 2013, **49**, 1440; B. Wu, H. Song, J. Zhou and X. Chen, *Chem. Commun.*, 2011, **47**, 8653.
- P. Wu, N. Du, H. Zhang, C. Zhai and D. Yang, *ACS Appl. Mater. Int.*, 2011, **3**, 1946.
- W. Qiu, J. Jiao, J. Xia, H. Zhonga and L. Chen, *RSC Adv.*, 2014, **4**, 50529.
- K. S. Pahari, A. Sinhamahapatra, N. Sutradhar, H. C. Bajaj and A. B. Panda, *Chem. Commun.*, 2012, **48**, 850; S. K. Pahari, P. Pal, D. N. Srivastava, S. C. Ghosh and A. B. Panda, *Chem. Commun.*, 2015, **51**, 10322; S. K. Pahari, N. Sutradhar, A. Sinhamahapatra, P. Pal, A. B. Panda, *New J. Chem.*, 2011, **35**, 1460
- N. Pradhan, Beni Katz and S. Efrima, *J. Phys. Chem. B*, 2003, **107**, 13843;
- Z. Lin, J. J. Cai, L. E. Scriven and H.T. Davis, *J. Phys. Chem.*, 1994, **98**, 5984.
- Q. H. Wang, K. Kalantar-zadeh, A. Kis, J. N. Coleman and M. S. Strano, *Nat. Nanotechnol.*, 2012, **7**, 699.
- M. Chhowalla, H. S. Shin, G. Eda, L.-J. Li, K. P. Loh and H. Zhang, *Nat. Chem.*, 2013, **5**, 263.
- T. Stephenson, Z. Li, B. Olsen and D. Mitlin, *Energy Environ. Sci.*, 2014, **7**, 209.
- K. Chang, W. Chen, L. Ma, H. Li, H. Li, F. Huang, Z. Xu, Q. Zhang and J.-Y. Lee, *J. Mater. Chem.*, 2011, **21**, 6251; K. Chang and W. Chen, *J. Mater. Chem.*, 2011, **21**, 17175; Z. Wang, T. Chen, W. Chen, K. Chang, L. Ma, G. Huang, D. Chen and J. Y. Lee, *J. Mater. Chem. A*, 2013, **1**, 2202; X. Zhou, L.-J. Wan and Y.-G. Guo, *Chem. Commun.*, 2013, **49**, 1838; X. Zhou, L.-J. Wan and Y.-G. Guo, *Nanoscale*, 2012, **4**, 5868.
- K. Bindumadhavan, S. K. Srivastava and S. Mahanty, *Chem. Comm.*, 2013, **49**, 1823.
- Y. Liu, Y. Zhao, L. Jiao and J. Chen, *J. Mater. Chem. A*, 2014, **2**, 13109; K. Zhang, H.-J. Kim, X. Shi, J.-T. Lee, J.-M. Choi, M.-S. Song and J. H. Park, *Inorg. Chem.*, 2013, **52**, 9807.
- H. J. Yoo, A. P. Tiwari, J. T. Lee, D. Kim, J. H. Park and H. Lee, *Nanoscale*, 2015, **7**, 3404; L. Hu, Y. Ren, H. Yang and Q. Xu, *ACS Appl. Mater. Interfaces*, 2014, **6**, 14644.
- M. Wang, G. Li, H. Xu, Y. Qian and J. Yang, *ACS Appl. Mater. Interfaces*, 2013, **5**, 1003.
- X. Fang, X. Yu, S. Liao, Y. Shi, S. Y. Hu, Z. Wang, D. G. Stucky and L. Chen, *Micropor. Mesopor. Mat.*, 2012, **151**, 418. D. G. Du, P. Z. Guo, S. Q. Wang, R. Zeng, Z. X. Chen and H. K. Liu, *Chem. Commun.*, 2010, **46**, 1106.
- U. K. Sen, P. Johari, S. Basu, C. Nayak and S. Mitra, *Nanoscale*, 2014, **6**, 10243.